Evaluation of the benefits of combined reflection and transmission hyperspectral imaging data through disease detection and quantification in plant-pathogen interactions

Stefan Thomas[1], Jan Behmann[2], Uwe Rascher[3], Anne-Katrin Mahlein[4]

Corresponding author: Anne-Katrin Mahlein, Mahlein@ifz-goettingen.de

Adresses:

1 Department of Phytopathology (360a), Institute of Phytomedicine (360), University of Hohenheim, 70599, Stuttgart, Germany

2 INRES Plant Disease, University of Bonn, 53115, Bonn, Germany (at time of contribution)

3 IBG2: Plant Sciences, Research Centre Jülich, 52428, Jülich, Germany

4 Institute of Sugar Beet Research (IfZ), 37079, Göttingen, Germany

Abstract:

Previous studies investigating the performance of transmission and reflection datasets for disease detection showed inconsistent results. Within the studies the performance of transmission imaging varied significantly for the detection of biotroph and necrotrophy plant pathogens, while reflection imaging showed excellent results in both studies. The current study explores the hypothesis that the disparity between these results might be correlated with the different interactions of the respective pathogens with the host plants and the way light interacts with the plant tissue. *Pyrenophora teres* f. *teres* and *Puccinia hordei* – the causative agents of net blotch and brown rust in barley – have been investigated with focus on early-stage detection

and quantification (disease severity) of symptoms. Datasets of hyperspectral imaging time-series measurements were analysed through application of multiple data analysis methods (support vector machines; principal component analysis with following distance classifier; spectral decomposition) in order to compare the performance of both datasets for the detection of disease symptoms.

It could be shown that transmittance-based brown rust detection (e.g., 12% disease severity) is outperformed by reflectance-based detection (e.g., 36% disease severity) regardless of the algorithm. However, both the detection and quantification of brown rust through transmittance was more accurate than those of powdery mildew in earlier studies. Transmittance and reflectance performed similar for the detection of net blotch disease during the experiments (~1% disease severity for reflection and transmission). Each data analysis method outperformed manual rating in terms of disease detection (e.g., 15% disease severity according to manual rating and 36% through support vector machines for rust reflection data). Except for the application of a distance classifier on net blotch transmittance data it could be shown, that pixels, which were classified as symptomatic through the data analysis methods while estimated to represent healthy tissue during manual rating, correlate with areas at the edges of manually detected symptoms. The results of this study support the hypothesis that transmission imaging results are highly correlated to the type of plant-pathogen interaction of the respective pathogens, offering new insights into the nature of transmission-based hyperspectral imaging and its application range.

Keywords: *Puccinia hordei*, *Pyrenophora teres* f. *teres*, data analysis, disease detection, hyperspectral imaging, reflectance, transmittance.

Introduction:

The use of optical sensors for plant phenotyping and detection of both abiotic and biotic stresses has become increasingly common as a research focus (Roitsch *et al*. 2019; Mahlein *et al*. 2019; Oerke 2020). However, the overwhelming majority of current studies are focussed on measuring the properties of light which is reflected from the plant tissue in order to correlate changes with plant stress reactions (Kuska *et al*. 2015; Alisaac *et al*. 2018; AlSuwaidi *et al*. 2018). Meanwhile research into the possibilities of the spectral properties of light which has been transmitted through the plant tissue is rarely conducted (Zhang *et al*. 2016; Hovi *et al*. 2018; Sun *et al*. 2018). Recent studies about the possibilities of transmitted light for plant pathogen detection with hyperspectral imaging sensors showed inconsistent results.

Thomas *et al*. (2017) performed a measurement of combined reflection and transmission with focus on plant-pathogen interaction with hyperspectral imaging sensors. The authors investigated barley leaves, which were inoculated with conidia of *Blumeria graminis* f. sp. *hordei* – the causative agent of powdery mildew – with the HyperArt measurement setup (Bergsträsser *et al*. 2015) for simultaneous measurement of reflection and transmission. The results of the study showed that it is possible to detect powdery mildew infection of barley leaves at leaf level two days before symptoms are visible on RGB images through automatically analysed reflection based hyperspectral data. Furthermore, it could be shown, that the combination of reflection and transmission data was advantageous to distinguish late powdery mildew symptom and spontaneous necrosis of resistant barley leaves. However, the results of the study did show that transmission-based detection of powdery mildew symptoms was not possible before symptoms on the leaves were already visible for two days with reflection based RGB imagery. These results stood in contrast to the study of Bergsträsser *et al*. (2015), which performed single measurements of visible symptoms of *Cercospora beticola* infection on sugar beet leaves. It was shown, that reflection and transmission-based data performed equally for the

detection of disease symptoms. Thomas *et al*. (2017) theorised, that this could be explained based on the different interaction of the two pathogens with the plant tissue. While powdery mildew symptoms, caused by the biotroph pathogen *Blumeria graminis* f. sp. *hordei*, develop as small pustules on the leaf surface with the fungi only penetrating the epidermis cells of the plant (Bhat *et al*. 2005; Dean *et al*. 2012), *Cercospora* leaf spot symptoms, caused by the necrotroph pathogen *Cercospora beticola*, appear as necrotic lesions on the leaves once the fungi switches to its necrotic phase after penetrating the leaf tissue through the stomata and spreading intercellularly (Steinkamp *et al*. 1979; Rangel *et al*. 2020). In this article further studies into the matter and principle of transmission measurement via optical sensors are presented in an attempt to confirm the hypothesis of Thomas *et al*. (2017).

Light interacts with plant leaves in a complex matter. Upon reaching the plant surface (cuticle and epidermis) a significant portion of the light is directly reflected and can be measured, providing information about the plant surface it interacted with (Fig. 1). The portion of the light which is neither reflected nor absorbed by the plant's surface enters the plant tissue, where it is scattered diffusely as it interacts with organelles and intercellular air spaces (Vogelmann *et al*. 1989). During the passing of the plant tissue a small amount of light is reflected back to the upper surface, the majority of light travels through the plant's mesophyll layer and the lower epidermis of the leaf. Upon reaching the surface-air border the majority of the diffusely scattered light is reflected back into the plant, with only a small portion is being transmitted through the leaf as it arrives at the surface-air border in the right angle (Fig. 1; Brakke 1994). The light, which was reflected is scattered diffusely once more as it travels back through the plant tissue layers up to the surface-air border of the upper epidermis, where a small portion is being transmitted and measured together with the surface reflection by reflection-based imaging methods, while the larger portion of the light is reflected back into the leaf tissue again (Fig. 1). This complex process allows the plant to maximize the usage of incoming light for

97 photosynthesis (Brakke 1994). These processes provide the reason why it is possible to detect
98 metabolic changes in plants with reflection-based measurement. The study of Nansen (2018)
99 did also show that hyperspectral measurements have a considerable penetration of measured
100 objects. Their study showed that different backgrounds influence leaf measurements –
101 especially with multiple layers of leaves being measured.

102 This could explain why reflection measurement outperforms transmission measurement for
103 biotroph pathogens like *Blumeria graminis* f. sp. *hordei*, which mostly interact with the plant
104 at the epidermis layer, as direct reflection at the plant surface permits the detection of the fungal
105 tissue. Meanwhile transmitted light would mix with light, which has not interacted with fungal
106 tissue or affected epidermis cells, due to diffuse scattering while traversing the leaf tissue,
107 reducing the detection efficiency. Necrotroph pathogens like *Cercospora betilola* tend to be
108 more invasive in their interaction with the host plant, which would result in a similar detection
109 accuracy to biotroph pathogens in reflectance measurement, but an increased performance in
110 transmittance measurement, as the traversing light interacts with the pathogen and infected
111 plant tissue in deeper layers of the leaf.

112 This study aims to provide insights into the matter of transmittance measurements of plant-
113 pathogen interaction through practical experiments with a set of pathogens with diverse
114 lifestyles. Measurements with the HyperArt setup were performed with barley leaves inoculated
115 with pathogens, which interact with different layers of the plant tissue, as time-series
116 measurements.

117 *Puccinia hordei*, the causative agent of brown rust, is a biotrophic pathogen, which enters
118 infected barley leaves through the stomata (Fig. 2b; Voegele 2006). Once inside the plant
119 mesophyll the fungi grows, forming intercellular haustoria to feed upon the plant before finally
120 forming colonies, which break through the epidermis to release new spores (Fig. 2b; Voegele
121 2006).

Pyrenophora teres f. *teres* (anamorph: *Drechslera teres*), the causative agent of net blotch, is a necrotrophic pathogen. It penetrates directly through the cuticle, cell wall and cell membrane of the host plants epidermis cells, where it forms a primary and secondary intracellular vesicle (Fig. 2c; Liu *et al*. 2011). When the secondary vesicle is formed, the host epidermis cell – as well as nearby epidermis cells – are functionally disrupted. A hypha forms intracellular from the secondary vesicle and breaks into the intercellular space of the mesophyll, where it secretes toxins/effectors which lead to the disruption of nearby mesophyll cells to provide the necrotrophic fungi with nutrients (Fig. 2c; Liu *et al*. 2011).

The two pathogens interact in a different way compared to *B. graminis* f. sp. *hordei*. The development of *P. hordei* is relatively subtle at first – before the plant tissue gets disrupted through the fungi breaking through the epidermis. Its growth within the mesophyll should allow for increased detection with transmission-based imaging, due to a reduced effect of the light scattering at pathogenic structures deeper within the leaf tissue. *P. teres* f. *teres* causes rapid cell death, which should result in similar results as the measurement of spontaneous necrosis in the study of Thomas *et al*. (2017) and should be comparable with the characteristic necrotic lesions in the centre of *Cercospora beticola* symptoms, which were investigated by Bergsträsser *et al*. (2015).

Through this approach – while taking into account the results of previous articles in regards to performance of reflectance and transmittance datasets – it should be possible to shed light on the performance of transmission imaging based on the differing plant-pathogen interactions of biotroph and necrotrophy pathogens. Multiple data analysis methods (both supervised and unsupervised) have been applied to the respective datasets in order to minimize the potential impact on disease detection accuracy. Thereby, observed differences between the performance of reflection and transmission datasets can be attributed to the different host-pathogen

interactions of the investigated diseases. The use of an unsupervised data analysis method and its comparison with the presented supervised methods is especially promising, as it does not rely on training data and thereby can both reduce workload and the potential for human error during data labeling.

Materials and Methods:

Plant cultivation and pathogen material

Hordeum vulgare L. cv. Ingrid wild type (Hinze *et al*. 1991) plants were grown in TEKU VQB 7x7x8 cm pots (Pöppelmann, Lohne, Germany) and filled with commercial substrate (Klasmann-Deilmann GmbH, Geeste, Germany) inside a climate chamber at 20/20 °C (day/night) 60% relative humidity (RH) and day light period of 16 h. At growth stage 12 according to BBCH scale (Hack *et al*. 1992) the plants were inoculated with the respective pathogens and placed in high humidity environment (>90%) and indirect lighting conditions for two days to maximize chance of infection before the second leaf of each plant was fixed within a custom plastic frame. 12 plants were used as healthy control, being inoculated with water, 12 plants were inoculated with a spore suspension (60000 spores/ml; spores were collected from infected wheat plants and stored at -80 °C to be used for inoculation directly after thawing) of *P. hordei* (stored field isolate from the area near Bonn) and 6 plants were inoculated through placement of cut leaves, showing heavy symptoms of *P. teres* f. *teres* infection, gathered around the area of Bonn. The inoculations were performed by spraying the spore suspensions and placing leaf pieces equally over the to be inoculated plant leaves for the two days the plants spend under high humidity conditions.

Hyperspectral imaging measurement

The HyperArt system was used to measure reflection and transmission of the plants simultaneously during the experiment (Bergsträsser *et al*. 2015; Thomas *et al*. 2017; Patent nr: DE102012005477). The system was modified according to Thomas *et al*. (2017). All leaves were measured in the visible and near infrared areas of the electromagnetic spectrum (400 – 1050 nm) in a daily time-series measurement from 3 days after inoculation (dai) to 9 dai. Measurements at earlier times were not possible, due to the requirement of the fungi to have high humility for infection of barley leaves. The leaves were kept fixated within the custom plastic frames over the entire measurement period to ease comparison of disease development at different images in the time series for data analysis. For each measurement a 99% reflectance white standard (Spectralon, Labsphere Inc., North Dutton, NH, USA) and a white diffuser lambertian transmission foil (Zenith Polymer® ≈ 50% transmission, SphereOptics GmbH, Uhldingen, Germany) was acquired, before measuring the leaf sample. These measurements served as white references for reflection and transmission images for the image normalization (Bergsträsser *et al.* 2015). Wavelength dependent differences in the percentage of the reflected and transmitted light of the two white references were taken into consideration during the normalization process. With each measurement a dark current image of the internal camera noise was measured by closing an internal camera shutter.

Data analysis

The reflectance and transmittance of the images was calculated by normalising the acquired images over the according white references, serving as standards with known reflection/transmission values, with ENVI 5.1 + IDL 8.3 (ITT Visual Information Solutions, Boulder, CO, USA). The normalized images were smoothened through the application of the Savitzky-Golay filter (Savitzky and Golay 1964) to eliminate noise within the hyperspectral datasets for further analysis. Background masking and separating the hyperspectral images to

196 single leaves was performed through an automated algorithm (thresholding based on global
197 average). In contrast the transmission images required manual extraction due to their spectral
198 properties being indistinguishable at places where parts of the frame were covering the plants
199 in order to hold them in place. Due to significant noise within the data at the extremes of the
200 sensor range the analyzed spectral range was reduced to 450 – 1000 nm.

201 The collected datasets of reflection- and transmission-based leaf images with developing net
202 blotch and brown rust symptoms respectively were analysed with three different data analysis
203 algorithms – support vector machines (SVM, Cortes and Vapnik 1995), spectral decomposition
204 (SD, Keshava and Mustard 2002) and a combination of principal component analysis (PCA)
205 with following distance classifier (DC, Mahalanobis *et al.* 1996). The SVM represents a
206 supervised approach of data analysis, in which a set of generated training data is used as basis
207 for classification. The SD is an unsupervised method, which generates classes based on distinct
208 datapoints within the analyzed dataset. The combination of PCA and DC finally represents a
209 mixed approach of reducing data dimensionality with the unsupervised PCA and sorting the
210 resulting correlation of pixels with the principal components into pre-generated classes with the
211 supervised DC. Classification results of data analysis approaches are investigated in
212 combination with manual rating (MR) to compare the potential of both the reflection and
213 transmission datasets for the characterization and detection of differing plant-pathogen
214 interactions.

215 In order to prepare the dataset for analysis of its variance with principal component analysis all
216 spectral signatures were normalized into the unit Euclidian norm to eliminate the influence of
217 non-biologic variance to the measurement. Thereby the signatures/vectors are treated as points
218 on a high dimensional unit sphere (Dhillon and Modha 2001; Leucker *et al*. 2016*b*), capturing
219 the vectors direction while reducing the variance in the dataset. After these preparations the
220 PCA was performed. PCA is a statistical method which introduced a new axis along the greatest

variance into the dataset, thereby transforming it based onto the variance and reducing the data complexity (Wold *et al*. 1987). The PCAs were performed over the healthy control leaves and the respective inoculated leaves within the dataset, including both reflection and transmission-based images. A supervised classification to determine disease symptoms on the leaves was performed through the application of the DC algorithm (Minimum distance classifier with centroid match method and Euclidian distance) on the results of the PCA. The DC uses a set of training data in order to classify every pixel of the image based on its distance in the Euclidian space from known classes.

An independent analysis of the data was performed by applying a non-linear support vector machines algorithm on the normalized dataset, which was used for the PCA with following DC. The applied SVM used radial basis function as kernel function to determine linear discriminant functions.

The DC and SVM were both trained with a set of labelled training data, which was generated by an expert, using control- and inoculated leaf images of six healthy and six inoculated leaves respectively at 7 dai from rust and net blotch datasets in order to classify both early and late stages of disease symptoms. Each leaf within the dataset averaged between 9000 and 14000 pixels, with the selected training data for each generated class averaging between 50 and 500 pixels, based on class rarity within the images. The manually annotated data was ordered into 14 classes (brown rust symptoms (early/late, reflection/transmission); net blotch symptoms (early/late, reflection/transmission); healthy tissue (leaf surface1/leaf surface2/leaf vein/leaf tip, reflection; leaf surface1/leaf vein, transmission)) and used as reference within the above classifications. Classes, which referred to healthy plant tissue of their respective datasets have been combined and are shown as one color in the result section, due to the focus on disease detection over slight differences in leaf reflection/transmission within different part of the leaf. For the comparison with manual rating and the manual rating itself the classes were simplified

to symptomatic and healthy tissue for their respective datasets, as a precise differentiation for each pixel into different disease stages or via the human eye and without the consultation of spectral signatures for the pixels was not feasible.

Finally, unsupervised spectral decomposition – based on the mixed pixel approach – was used to analyze the datasets. Spectral decomposition factorizes the matrix, which is made up of the to be analyzed hyperspectral dataset, into a canonical form, representing it in terms of its eigenvalues and eigenvectors. This algorithm was applied unsupervised, with the program selecting mixed pixels of the image so as to determine the eigenvalues. The abundance of these eigenvalues within the dataset was then calculated to give out both an abundance map with abundance per pixel, as well as a classification of the image over the generated classes.

The data analysis methods were performed with the FluxTrainer 2.9.0.1 Software (LuxFlux GmbH, Reutlingen, Germany).

Leaves were manually rated by an expert at the end of the experiment 9 dai. The manual rating was performed with a Pseudo RGB image as basis with the goal to label healthy and infected leaf tissue. Unlike the generated training data, each pixel of the images was sorted into the classes healthy and symptom during this rating to compare disease severity visible by eye with the results of the different data analysis methods. Pixels that showed clearly identifiable disease Symptoms with the bare eye were labelled as Symptom, while other pixels were labelled as healthy.

The results of the manual rating were used as comparison for post classification of the data. This was achieved via a two-ways approach. The leaf images of different dates were compared with each other in order to determine if the classification results which showed pixels as diseased without visible symptoms correlate with symptom development at later dates (Fig. 3 and 4). Furthermore, the classifiers and MR were analyzed through confusion matrices of the classification results from the different data analysis methods on both reflection and

transmission datasets. Confusion matrices were computed via a C++ program. The results of the confusion matrices were visualized (see fig. 7 and 8) to determine if the grouping of pixels that were classified as symptomatic in the algorithms but not the MR correlate with the expected development of disease symptoms to further validate the data analysis.

Results:

Manual assessment of the gathered datasets

The water-inoculated control plants did not show any development of disease symptoms of either net blotch or brown rust over the course of the experiment.

The plants which were inoculated through direct contact to leaf pieces, infected with *P. teres* f. *teres*, developed net blotch symptoms. First symptoms of the net blotch disease became visible at 5 dai both in reflection- and transmission-based images and slowly progressed until the last measurements were taken at 9 dai (Fig. 3). During this time the symptoms developed from the initially infected areas of the host plants leaves, which had direct contact with infected leaf parts during inoculation. Throughout the symptom development the net blotch symptoms proved to be equally visible in reflection and transmission images, showing similar leaf discoloration and symptom area (Fig. 3). During manual rating of the disease severity at 9 dai the reflection and transmission data were rated with 0.72 and 0.69 percent of the leaf area showing symptomatic tissue respectively (Table 1).

The plants which were inoculated with *P. hordei* (*Ph*) spore suspension developed without exception brown rust symptoms over the course of the experiment. First disease symptoms became visible at 5 dai in the reflection-based images and 6 dai in the transmission-based images – with the symptoms being easier to distinguish in the reflection-based data (Fig. 4). Symptoms developed over the entire leaf area, starting with discrete, small chlorotic spots at

295 the initial infection sites. Typical yellow, chlorotic areas were forming on the leaves at 5 dai
296 and growing, with brown spore colonies breaking through the epidermis and becoming visible
297 from 7 dai until the end of the experiment – this process could be clearly observed in the
298 reflection-based images (Fig. 4). Meanwhile, in the transmission-based images this process
299 could only be observed as a slight darkening of the symptomatic leaf areas, which became
300 visible at 6 dai, and the development of brown spots in the middle of the described darkened
301 areas, starting at 7 dai (Fig. 4). During manual rating of disease severity – based on reflection
302 and transmission datasets – 15.25 and 5.04 percent of the leaf tissue was rated as symptomatic
303 tissue respectively (Table 1).

304

305 *Analysis of the respective reflection- and transmission-based data through three distinctive*
306 *data analysis methods*

307 The datasets for the investigated pathogens – for both reflectance and transmittance data – were
308 analysed with the three distinct data analysis methods (SVM, DC, SD), as described above.

309 The leaf images of the control plants were classified as healthy tissue for both reflectance and
310 transmittance with the exception of <0.1% of the pixels, which were classified as disease
311 symptoms for SVM and SD classification. The falsely classified pixels were located either at
312 the edge of the leaves or in the areas where the frame was covering parts of the leaves during
313 measurement (Fig. 5). Thereby, containing mixed information of the respective
314 reflected/transmitted light of both the measured leaf and the black background/frame. The DC
315 algorithm – based on the results of the previously performed PCA – performed noticeably
316 worse, having overall the highest tendency to falsely classify pixels in the above-mentioned
317 areas with up to 0.3% of pixels being falsely classified as symptoms. The DC classification also
318 was unable to differentiate between symptoms and the leaf vein in the transmission-based

images of the net blotch dataset, causing pixels of the leaf veins to be classified as disease symptom, increasing the falsely classified pixels up to 10% in this specific case (Fig. 5).

Both DC and SD algorithms were able to detect net blotch symptoms within the reflectance images of the inoculated leaves at 4 dai – one day before the symptoms were visible with the human eye – and able to track the development of the symptoms during the following measurement days, whereby the DC did show a clearer detection of early symptoms but was also more prone to misclassify pixels containing healthy tissue as symptoms (Fig. 3). For transmission-based images the algorithms were able to detect first net blotch symptoms at 5 dai, showing a slightly reduced performance in early disease detection compared to reflectance-based data (Fig. 3). The SVM based classification performed notably worse for early detection in reflection-based images. Despite using the same training data set as the DC first symptoms were only detected at 7 dai. Meanwhile, the transmittance images allowed a detection of the symptoms at 5 dai, performing similar to the other two algorithms (Fig. 3).

At 9 dai, the final measurement day for the experiment, net blotch symptoms could be classified by all three data analysis methods in both reflectance and transmittance images, correlating with the results of manual labelling of disease symptoms – both in disease severity (Table 1) and location of disease symptoms on the leaf (Fig. 5). A notable exception being the DC algorithm for the transmission-based image, as the above-mentioned classification error of the leaf vein persists, causing a disparity of about 10% in disease severity compared to manual rating results and other methods.

When looking in more detail at the classification of the specific pixels within the images through the application of confusion matrices with the manual rating serving as the standard method for comparison of the different classification results with classic disease detection approaches. In order to achieve this one leaf for ach pathogens was manually rated, with the leaf for brown rust consisting of 13048 and the one for net blotch of 13418 manually annotated

pixels. The results show, that all three algorithms have a high accuracy for the correct classification of healthy tissue and symptoms within the reflection data (89.6% for SVM and 84.5% for SD), with the DC algorithm outperforming the other two for disease detection (100%; Table 2). Within the transmission dataset the accuracy of all three algorithms is reduced (78.4% for SVM, 70.1% for SD and 97.9% for DC), with DC showing an uncharacteristically high error margin for misclassification of healthy tissue (10.6%) due to the misclassification of pixels showing the leaf vein as symptoms (Table 2).

Within the brown rust dataset, the SVM classified first pixels in reflectance images as disease symptoms at 4 dai, one day before the disease became visible with the human eye, and classifies symptomatic leaf areas correctly over the course of the experiment (Fig. 4). In the transmission-based images the SVM only detects disease symptoms at 6 dai. Due to high difficulties in differentiating early disease symptoms and healthy tissue it was however necessary to create multiple classes of healthy leaf tissue within the training data for both SVM and DC. As wheat leaves are not entirely homologous in their reflection and transmission properties – based on leaf age, leaf structures, leaf angle, etc. – and the early pathogen signatures being similar to those of the control leaves multiple distinct classes at different pathogen stages and at healthy leaf areas with specific features have been created. This explains the early misclassification of pixels showing healthy leaf tissue as disease symptoms at 4 dai for the DC (Fig. 4). As shown in figure 4 the DC classification increases in accuracy over the course of the experiment, correlating significantly better with the results of the other data analysis methods at 8 and 9 dai (36% / 12% for SVM reflectance / transmittance, 38% / 21% for DC reflectance /transmittance). When applied to the transmittance images the DC does not have these issues, accurately detecting disease symptoms from 6 dai onwards like the SVM. The transmission-based dataset could be classified with only a single class for healthy tissue, showing a more uniform spectral signature over the leaf area when compared with the reflectance dataset. Disease symptom

detection with the SD classified first disease symptoms at 5 dai and 6 dai for reflectance and transmittance images respectively and shows accurate detection over the course of the experiment (Fig. 4), with a slightly reduced disease severity assessment compared to SVM and DC (27% /14% for reflectance / transmittance).

Comparison of the classification results at 9 dai shows that all data analysis algorithms achieve significantly higher disease severity ratings then manual rating for both reflectance (e. g. 36% for SVM compared to 15% for manual rating (brown rust)) and transmittance (e. g. 12% for SVM compared to 5% for manual rating (brown rust)) datasets (Table 1), while the spatial distribution of symptomatic pixels within the images matches for data analysis methods and manual rating (Fig. 6).

The post classification results of the respective confusion matrices show that the selected algorithms are able to accurately detect disease symptoms, which were labelled in the manual rating, in both reflection (97% for SVM, 86.3% for DC, 88.3% for SD) and transmission (86% for SVM, 95.5% for DC, 92.3% for SD) data (Table 2). The detection accuracy of the SVM for reflectance images being notably higher than other algorithms. Both DC and SD have a higher accuracy for transmittance image symptom detection, while the accuracy of the SVM decreases when compared with the results of reflection data. All algorithms classified a high percentage of pixels which did not show clearly visible disease symptoms – and where thereby marked as healthy tissue in the manual rating – as symptoms (25.8% for SVM, 30.4% for DC, 16.5% for SD) for the reflectance images, while the results of the transmittance images show a lower error margin (Table 2).

Discussion:

392 The results of this study show differences within the performance of transmission-based
393 measurement approaches, depending on the way pathogens interact with the host plant. Within
394 this study the biotroph pathogen *Puccinia hordei* and the necrotroph pathogen *Pyrenophora*
395 *teres* f. *teres* have been investigated with both reflection and transmission measurement
396 approaches. Combined with the results of Thomas *et al*. (2017), which investigated the
397 reflection and transmission-based detection of the biotroph pathogen *Blumeria graminis* f. sp.
398 *hordei* and theorized the low performance of transmission data was related to the interactions
399 of light with the tissue while passing the leaf, this allows the estimation of cases in which the
400 addition of transmission-based approaches would be beneficial for increased accuracy in
401 disease detection. B. graminis f. sp. hordei mainly interacts with the epidermis layer of the plant,
402 while P. hordei – albeit also a biotroph pathogen – grows into the intercellular space and
403 interacts with cells within the mesophyll layer (Fig. 2). The necrotoph pathogen *P. teres* f. *teres*
404 secretes mycotoxins, which cause necrosis over all layers of the leaf tissue in areas where the
405 mycelium of the pathogen is present (Fig.2). This study provides insights about the interaction
406 of transmitted light with the different pathogens and thereby its potential for disease detection,
407 based on the performance of transmission measurement for the detection and quantification of
408 the pathogens with their differing host-pathogen interactions and the comparison to reflection-
409 based measurement.

410

411 *Evaluation of transmission-based imaging data for disease detection*

412 The theory postulated by Thomas *et al*. (2017) that light scattering within the leaf influences
413 the disease detection through transmittance images and thereby the interactions of pathogens
414 with the host plant play an important role in detection speed and accuracy is supported by the
415 results of the current study.

It could be shown that net blotch symptoms are detected with no substantial differences in disease severity at later stages. This was true for both manual rating of reflectance and transmittance images, as well as classification results with SVM and SD (Table 1). The combination of PCA and DC did classify a notably higher number of pixels in the transmittance data as diseased, this can be explained due to the inability of the algorithm to discern pixels showing the leaf veins from pixels with disease symptoms (Table 2). Figure 7 shows, that the majority of pixels which were classified as showing symptoms in the transmission images of the DC results while being labelled as healthy in the MR align with the leaf vein placement on barley leaves. These results coincide with the findings of Bergsträsser *et al*. (2015), which investigated the advantages of combined reflectance and transmittance measurements for disease severity estimation on developed *Cercospora* leaf spot symptoms via a comparison of *Cercospora* leaf spot index results derived from reflectance and transmittance images. Like the net blotch disease, which was investigated in this study, *Cercospora* leaf spot disease also causes necrotic lesions on infected sugar beet leaves (Mahlein *et al*. 2012, Leuker *et al*. 2016). The results of both studies also correlate with findings of Thomas *et al*. (2017) that transmission-based images allowed for precise detection of spontaneous necrosis on leaves and their differentiation from late stage powdery mildew symptoms, which required more complex methodology when differentiated through reflection-based data.

In contrast the estimation of disease severity of brown rust on barley leaves within this study showed, that the estimates based on transmittance images were lower compared to reflectance image-based estimates (Table 1). The algorithms did each classify a significant number of pixels, which could not be labelled as symptomatic during the MR, into the symptoms group for both reflectance and transmittance images (Table 2). The location of these pixels shows, that they are mostly located at the outer edges of areas which were labelled as symptoms through MR, hinting at the possibility to detect brown rust infection before visible symptoms

appear at a given location (Fig. 8). Despite the success of the algorithms for disease detection it showed that the estimated disease severity in transmission-based images was significantly lower than reflection-based images, with MR and SVM showing the highest discrepancy of about 66% between the results – ~15% and ~35% disease severity for reflectance and ~5% and ~11% for transmittance respectively (Table 1). Visibility of brown rust symptoms with the human eye within the transmittance images was mostly limited to areas where spore colonies had formed and broken through the leaf epidermis, with chlorotic lesions from prior rust development being barely visible once larger areas were infected. Nevertheless, the detection of brown rust symptoms was more accurate and could be earlier detected within transmission-based data then the powdery mildew symptoms in the study of Thomas *et al*. (2017), in which powdery mildew symptoms were detected through principal component analysis. All used algorithms in the current study have shown to be able to detect disease symptoms one day after they became visible within the reflectance images (Fig. 4) compared to two days for powdery mildew in the previous study (see Thomas *et al* 2017, figure 6).

These findings show, that while pathogen detection through reflectance is similar for biotroph (*B. graminis*) and necrotroph (*C. beticola*) pathogens shown in earlier studies (Bergsträsser *et al*. 2015; Thomas *et al*. 2017), the detection efficiency through transmittance varies considerably for pathogens investigated in the current study. Necrotroph pathogens like net blotch (current study) and *Cercospora* leaf spot disease (Bergsträsser *et al*. 2015) can be detected equally well through reflection and transmission at late disease development stages. Meanwhile, for biotroph pathogens, such as brown rust (current study) and powdery mildew (Thomas *et al*. 2017), reflection-based pathogen detection outperforms transmission-based detection. Nevertheless, it could be shown that, when comparing the results of brown rust detection through transmittance data with the detection of powdery mildew symptoms in Thomas *et al*. (2017), the classification of brown rust symptoms through transmission-based

466 data analysis is more accurate and allows for earlier detection of the pathogen then those for
467 powdery mildew – with transmission imaging being able to detect powdery mildew two days
468 after symptoms could be detected through reflection imaging, while brown rust could be
469 detected with a delay of one day only. These trends can be explained by the interaction of
470 transmitted light with the plant tissue (Fig. 1). As the light becomes diffusely scattered while
471 traversing the leaf tissue it stands to reason that more intrusive pathogens, which interact with
472 deeper cell layers inside the leaf, would be less affected by these effects then pathogens which
473 interact with the plant surface and epidermis layers, such as powdery mildew (Fig. 9). As
474 necrotroph pathogens cause significantly more cellular damage then biotroph pathogens and,
475 like the example of net blotch shows (Fig. 2), interact with all layers of the leaf, it is reasonable
476 that they would be best suited for transmission-based detection. These findings support the
477 hypothesis of Thomas *et al*. (2017) that the differences in transmission-based disease detection
478 for selected pathogens is rooted in the nature of their interaction with the host plant and suggest
479 that transmission-based pathogen detection is correlated significantly with the intrusiveness of
480 a given pathogen during its development inside the host tissue.

481

482 *Early disease detection through transmission*

483 It has been shown by multiple studies that hyperspectral reflectance imaging sensors are able
484 to detect disease symptoms before symptoms are visible with the human eye (Kuska *et al*. 2015,
485 Thomas *et al*. 2017, Behman *et al*. 2018). So far this could not be shown for images based on
486 transmission, as studies with time-series measurements that compare the performance of
487 reflectance and transmittance hyperspectral images for early plant disease detection are, to the
488 knowledge of the authors, not available – besides Thomas *et al*. (2017). Within the study of
489 Thomas *et al*. (2017) powdery mildew infection could be detected based on transmittance

images at 6 dai, two days after detection was possible through the reflectance images and at a point when the disease symptoms were already visible by eye in reflection-based RGB images.

In the current study both net blotch and brown rust symptoms in transmittance images could be detected one to two days after detection was possible in reflectance images for all applied data analysis methods – with the notable exception of net blotch symptom detection through SVM, which can be explained as the SVM failed to detect symptoms in the reflection-based dataset before 7 dai while the two other algorithms managed to detect at 4 dai. While this exception shows that under certain circumstances it is possible to achieve earlier disease symptom detection through transmission-based images it would be more suited to use an algorithm that performs better for the detection of net blotch symptoms as the symptoms were visible by eye at 5 dai.

From the results of these studies, it can be concluded that transmission-based measurements are not well suited for early disease detection, even from highly invasive pathogens. A possible explanation would be that pathogens like net blotch spread from their entry point at the leaf surface (Fig. 2), which might cause changes within the plants spectral signature to be detected in reflectance images while the internal light scattering inside the leaves prevents detection of these early plant/pathogen interactions through transmission-based imaging (Fig. 9). While this effect would be reduced for more intrusive pathogens like brown rust and net blotch, it could cause an increase of mixed spectra – containing partial information of symptomatic and healthy leaf areas within a pixel due to internal light scattering – in the transmission data during early pathogen development in transmission measurement compared to reflection measurement.

Comparison of data analysis methods for disease detection and disease severity estimation within this study

514 Due to the relatively small size of the datasets, which were collected in the experiments it was
515 decided that – while deep learning approaches have recently shown to be promising in plant
516 stress detection (Golhani *et al*. 2018; Singh *et al*. 2018; Feng *et al*. 2020) – classical machine
517 learning methods would be applied within the current study. While the datasets consist of two
518 independent time series measurements per pathogen, containing 12 and 6 plants respectively
519 with thousands of pixels per leaf, it was deemed unlikely that the amount of data would be
520 sufficient for the requirements of deep learning approaches (Singh *et al*. 2018). Meanwhile
521 machine learning methods have shown excellent results for the analysis of optical data for the
522 estimation of plant parameters in the past, as well as recent studies (Wahabzada *et al*. 2015;
523 Heckmann *et al*. 2017; Ugarte Fajardo *et al*. 2020).

524 Three different data analysis methods have been used in this study and were compared to MR
525 of the RGB images in order to verify the results of the experiments and minimize the risk, that
526 the conclusions are adequate to investigate the characteristics of transmitted light for the
527 investigation of plant-pathogen interactions. In comparison with the MR every algorithm
528 achieved a higher disease severity estimation for both net blotch (Fig. 5) and brown rust (Fig.
529 6) symptoms both for reflectance and transmittance images (Table 1). These results, while
530 promising, are posing the question if the classifications of the different algorithms are correct,
531 or misclassifying pixels showing healthy tissue as symptomatic. To clarify this issue, the results
532 of each algorithm were investigated twofold. First the classification results of images early in
533 the time-series were compared with pseudo RGB images from later stages for both net blotch
534 (Fig. 3) and brown rust (Fig. 4) datasets. As the leaves were fixed during the entire timeframe
535 of the measurements it was possible to compare the placement of pixels within different
536 visibility stages. Furthermore, the results of the post classification through confusion matrices
537 compared to the MR were visualized for both net blotch (Fig. 7) and brown rust (Fig. 8) images
538 at 9 dai. These visualizations show, that the vast majority of the pixels which were classified as

showing symptoms through the data analysis are grouped around clusters of pixels that were labelled as symptomatic in the MR. It was expected that the different data analysis methods are able to classify pixels without symptoms being visible to the human eye, as it is one of the main interests in analysing hyperspectral imaging data to detect disease symptoms before they are visible by the human eye in RGB images (Behman *et al*. 2018).

Among the data analysis methods, the combination of PCA and DC showed the highest estimations of disease severity, but is also the method that has been shown to be most prone to mistakenly classify healthy tissue as symptoms for net blotch (transmission, Fig. 7) and brown rust (reflection, Fig. 8). In these cases, the SVM was able to clearly differentiate between disease symptoms and healthy tissue, while being trained on the same set of training data. The SVM as a supervised method performed well for both early detection and disease severity estimation, with the notable exception of net blotch reflectance images (Fig. 3). The unsupervised SD performed well in all cases, being able to detect symptoms as early as the supervised methods – with the exception of brown rust reflectance, where the SVM was able to detect symptoms one day prior to other methods (Fig. 4) – and was overall the least prone to misclassification. SD has the added advantage, that the unsupervised algorithm does not require training data in order to function and did classify disease symptoms and healthy tissue while generating fewer classes then the supervised methods required. However, the SD had in all cases the lowest disease severity estimates when compared with other algorithms, but still outperformed MR (Table 1).

The combination and comparison of the results of different data analysis algorithms ensured that no false conclusions through performance abnormalities of a single algorithm while investigating the properties of reflectance and transmittance datasets could occur. This was necessary, as it has been shown in earlier studies, that the accuracy of different machine learning methods can vary depending on the investigated dataset (AlSuwaidi *et al*. 2018; Barreto *et al*.

2020).While outliers in algorithm performance, such as the late detection of brown rust symptoms in reflectance images of SVM and the misclassification of leaf vein pixels as net blotch symptoms through DC, occurred it was possible to identify them through comparison with the alternative data analysis algorithms employed within the study.

Conclusion:

The postulated theory that the nature of the plant-pathogen interaction during pathogen infection is related to the possibility to detect disease symptoms through transmission-based imaging is being supported by the results of this study. Thereby, the use of transmission measurement is most suited for invasive pathogens, which cause tissue damage in deeper layers of the leaf, or in order to separate stress factors which show a high similarity within the changes to the spectral signature of reflectance data. Transmission-based measurements seem to be outperformed by reflection-based measurements in general when it comes to early disease detection.

Acknowledgements:

The authors would like to thank the members of the INRES-Plant Protection and Plant Diseases and IBG2: Plant Sciences for their support during the experiments and fruitful discussions. Furthermore, the authors would like to thank the reviewers for helpful comments and constructive critique of the article.

Experiments in this study were conducted at the INRES of the University of Bonn, as well as the IGB2: Plant sciences of the Research Centre Jülich as part of the CROP.SENSe.net program.

Declarations:

Funding

Funding was provided by the German Federal Ministry of Education and Research (BMBF) within the scope of the competitive grants program "Networks of excellence in agricultural and nutrition research—CROP.SENSe.net" (Funding code: 0315529), junior research group "Hyperspectral phenotyping of resistance reactions of barley", within the German-Plant-Phenotyping Network (project identification number: 031A053), and by the Daimler and Benz foundation.

Uwe Rascher and Anne-Katrin Mahlein are partially funded by the Deutsche Forschungsgemeinschaft (DFG, German Research Foundation) under Germany's Excellence Strategy - EXC 2070 – 390732324.

Conflicts of interest/Competing interests

Not applicable.

Availability of data and material

The datasets, which were generated and analysed during the study, are not publicly available due to their large sizes. However, they can be provided by the corresponding author upon request.

Code availability

609 Fluxtrainer and Envi software are commercially available. Matlab scripts can be provided by
610 the corresponding author upon request.

611

612 *Author's contributions*

613 ST, UR and AKM designed the study and refined the hyperspectral measurement system. ST
614 performed the hyperspectral measurements. ST and JB performed the statistical analysis. ST
615 drafted the manuscript with support from JB, UR and AKM. All authors read and approved the
616 final manuscript.

617

618 **References:**

619 Alisaac E, Behmann J, Kuska MT, Dehne H-W, Mahlein A-K (2018) Hyperspectral
620 quantification of wheat resistance to Fusarium head blight: comparison of two Fusarium
621 species. European Journal of Plant Pathology 152:869–884.

622 AlSuwaidi A, Grieve B, Yin H (2018) Feature-Ensemble-Based Novelty Detection for
623 Analyzing Plant Hyperspectral Datasets. IEEE Journal of Selected Topics in Applied Earth
624 Observations and Remote Sensing 11:1041-1055.

625 Behmann J, Bohnenkamp D, Paulus S, Mahlein A-K (2018) Spatial referencing of
626 hyperspectral images for tracing of plant disease symptoms. Journal of Imaging 4:143.

627 Bergsträsser S, Fanourakis D, Schmittgen S, Cendrero-Mateo MP, Jansen M, Scharr H, Rascher
628 U (2015) HyperART: non-invasive quantification of leaf traits using hyperspectral absorption-
629 reflectance-transmittance imaging. Plant Methods 11:1–17.

630 Bhat R, Miklis M, Schmelzer E, Schulze-Lefert P, Panstruga R (2005) Recruitment and
631 interaction dynamics of plant penetration resistance components in a plasma membrane

632 microdomain. Proceedings of the National Academy of Sciences of the United States of
633 America 102:3135–3140. doi:10.1073/pnas.0500012102

634 Barreto A, Paulus S, Varrelmann M, Mahlein A-K (2020) Hyperspectral imaging of symptoms
635 induced by *Rhizoctonia solani* in sugar beet: comparison of input data and different machine
636 learning algorithms. Journal of Plant Diseases and Protection 127:441–451.

637 Brakke TW (1994) Specular and diffuse components of radiation scattered by leaves.
638 Agricultural and Forest Meteorology 71:283–295.

639 Cortes C, Vapnik V (1995) Support-vector networks. Machine Learning 20:273–97.

640 Dean R, Van Kan JAL, Pretorius ZA, Hammond-Kosack KE, Pietro AD, Spanu PD, Rudd JJ,
641 Dickman M, Kahmann R, Ellis J, Foster GD (2012) The top 10 fungal pathogens in molecular
642 plant pathology. Molecular Plant Pathology 13:414–430. doi:10.1111/j.1364-
643 3703.2011.00783.x

644 Dhillon IS, Modha DS (2001) Concept decompositions for large sparse text data using
645 clustering. Machine Learning 42:143–175.

646 Feng X, Zhan Y, Wang Q, Yang X, Yu C, Wang H, Tang Z, Jiang D, Peng C, He Y (2020)
647 Hyperspectral imaging combined with machine learning as a tool to obtain high-throughput
648 plant salt-stress phenotyping. The Plant Journal 101:1448–1461.

649 Golhani K, Balasundram SK, Vadamalai G, Pradhan B (2018) A review of neural networks in
650 plant disease detection using hyperspectral data. Information Processing in Agriculture 5:354-
651 371.

652 Heckmann D, Schluter U, Weber APM (2017) Machine Learning Techniques for Predicting
653 Crop Photosynthetic Capacity from Leaf Reflectance Spectra. Molekular Plant 10:878-890.

654 Keshava N, Mustard JF (2002) Spectral Unmixing. IEEE Signal Processing Magazine 19:44-
655 57.

656 Hovi A, Forsström P, Mõttus M, Rautiainen M (2018) Evaluation of Accuracy and Practical
657 Applicability of Methods for Measuring Leaf Reflectance and Transmittance Spectra. Remote
658 Sensing 10(1):25. https://doi.org/10.3390/rs10010025

659 Kuska M, Wahabzada M, Leucker M, Dehne H-W, Kersting K, Oerke EC, Steiner U, Mahlein
660 A-K (2015) Hyperspectral phenotyping on the microscopic scale: towards automated
661 characterization of plant-pathogen interactions. Plant Methods 11:28.

662 Leucker M, Wahabzada M, Kersting K, Peter M, Beyer W, Steiner U, Mahlein A-K, Oerke E-
663 C (2016) Hyperspectral imaging reveals the effects of sugar beet QTLs on *Cercospora* leaf spot
664 resistance. Functional Plant Biology 44:1-9.

665 Liu Z, Ellwood SR, Oliver RP, Friesen TL (2011) *Pyrenophora teres*: Profile of an increasingly
666 damaging barley pathogen. Molecular Plant Pathology 12:1-19.

667 Mahalanobis A, Vijaya Kumar BVK, Sims SRF (1996) Distance-classifier correlation filters
668 for multiclass target recognition. Applied Optics 35:3127-3133.

669 Mahlein A-K, Steiner U, Hillnhütter C, Dehne H-W, Oerke E-C (2012) Hyperspectral imaging
670 for small-scale analysis of symptoms caused by different sugar beet diseases. Plant Methods
671 8:3.

672 Mahlein A-K, Kuska M, Thomas S, Wahabzada M, Behmann J, Rascher U, Kersting K (2019)
673 Quantitative and qualitative phenotyping of disease resistance of crops by hyperspectral
674 sensors: seamless interlocking of phytopathology, sensors, and machine learning is needed!.
675 Current Opinion in Plant Biology 50:156-162.

676 Oerke EC (2020) Remote sensing of diseases. Annual Review of Phytopathology 58:225–252

677 Rangel LI, Spanner RE, Ebert MK, Pethybridge SJ, Stukenbrock EH, de Jonge R, Secor GA,
678 Bolton MD (2020) *Cercospora beticola*: The intoxicating lifestyle of the leaf spot pathogen of
679 sugar beet. Molecular Plant Pathology 21:1020–1041. https://doi.org/10.1111/mpp.12962

680 Roitsch T, Cabrera-Bosquet L, Fournier A, Ghamkhar K, Jiménez-Berni J, Pinto F, Ober ES
681 (2019) Review: New sensors and data-driven approaches - A path to next generation
682 phenomics. Plant Science 282:2-10.

683 Savitzky A, Golay M (1964) Smoothing and differentiation of data by simplified least squares
684 procedures. Analytical Chemistry 36:1627–1639.

685 Singh AK, Ganapathysubramanian B, Sarkar S, Singh A (2018) Deep Learning for Plant Stress
686 Phenotyping: Trends and Future Perspectives. Trends in Plant Science 23:883-898.

687 Steinkamp M, Martin S, Hoefert L, Ruppel E (1979) Ultrastructure of lesions produced by
688 Cercospora beticola in leaves of Beta vulgaris. Physiological Plant Pathology 15:13–26.

689 Sun J, Kunnemeyer R, McGlone A, Tomer N (2018) Optical properties of healthy and rotten
690 onion flesh from 700 to 1000 nm. Postharvest Biology and Technology 140:1–10.

691 Thomas S, Wahabzada M, Kuska M, Rascher U, Mahlein A-K (2017) Observation of plant–
692 pathogen interaction by simultaneous hyperspectral imaging reflection and transmission
693 measurements. Functional Plant Biology 44:23–34.

694 Ugarte Fajardo J, Bayona Andrade O, Criollo Bonilla R, Cevallos-Cevallos J, Mariduena-
695 Zavala M, Ochoa Donoso D, Vicente Villardón JL. (2020) Early detection of black Sigatoka in
696 banana leaves using hyperspectral images. Applications in Plant Sciences 8:e11383.

697 Voegele RT (2006) *Uromyces fabae*: development, metabolism, and interactions with its host
698 *Vicia faba*. FEMS Microbiology Letters 259:165–173.

699 Vogelmann TC (1989) Penetration of light into plants. Photochemistry and Photobiology
700 50:895–902.

701 Wahabzada M, Mahlein A-K, Bauckhage C, Steiner U, Oerke E-C, Kersting K (2015) Metro
702 Maps of Plant Disease Dynamics—Automated Mining of Differences Using Hyperspectral
703 Images. PLoS ONE 10(1):e0116902. https://doi.org/10.1371/journal.pone.0116902

704 Wold S, Esbensen K, Geladi P (1987) Principal component analysis. Chemometrics and
705 Intelligent Laboratory Systems 2:37–52.

706 Zhang H, Salo D, Kim DM, Komarov S, Tai Y-C, Berezin MY (2016) Penetration depth of
707 photons in biological tissues from hyperspectral imaging in shortwave infrared in transmission
708 and reflection geometries. Journal of Biomedical Optics 21:126006.

709

Figures:

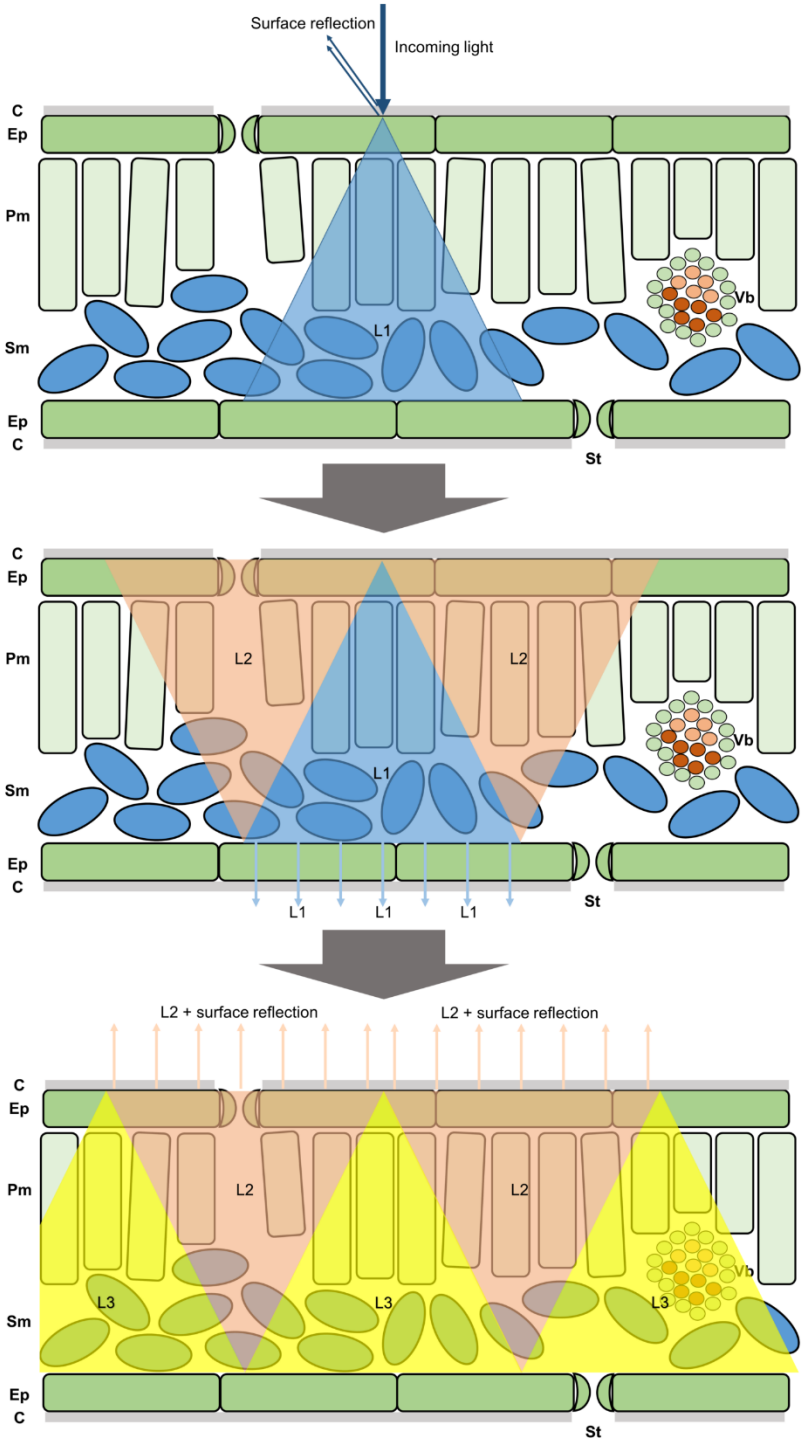

Fig. 1 Pathway of light when interacting with a plant leaf. Upon reaching the plant's surface a portion of the light is reflected back from the cuticle (C) and epidermis (Ep), while the rest of the light enters the plant tissue in a diffusely scattered manner (L1, blue cone). The light crosses both palisade- (Pm) and spongy mesophyll (Sm) - being partially absorbed and scattered back to the leaf surface as indirect reflection - before reaching the epidermis and

717 cuticle un the bottom of the leaf. Here a portion of the light is transmitted, thereby exiting the
718 leaf as transmitted light (L1, blue arrows), while the rest is being reflected at the leaf surface-
719 air border and traverses the mesophyll tissue again while being diffusely scattered (L2, orange
720 cones). Upon reaching the epidermis and cuticle of the top of the leaf a portion of L2 is
721 transmitted as indirect reflection and would be measured with the light coming from the
722 surface reflection, while the rest is reflected from the leaf surface-air border to continue its
723 path through the leaf (L3, yellow cones). St = stomata, Vb = vascular bundle

724

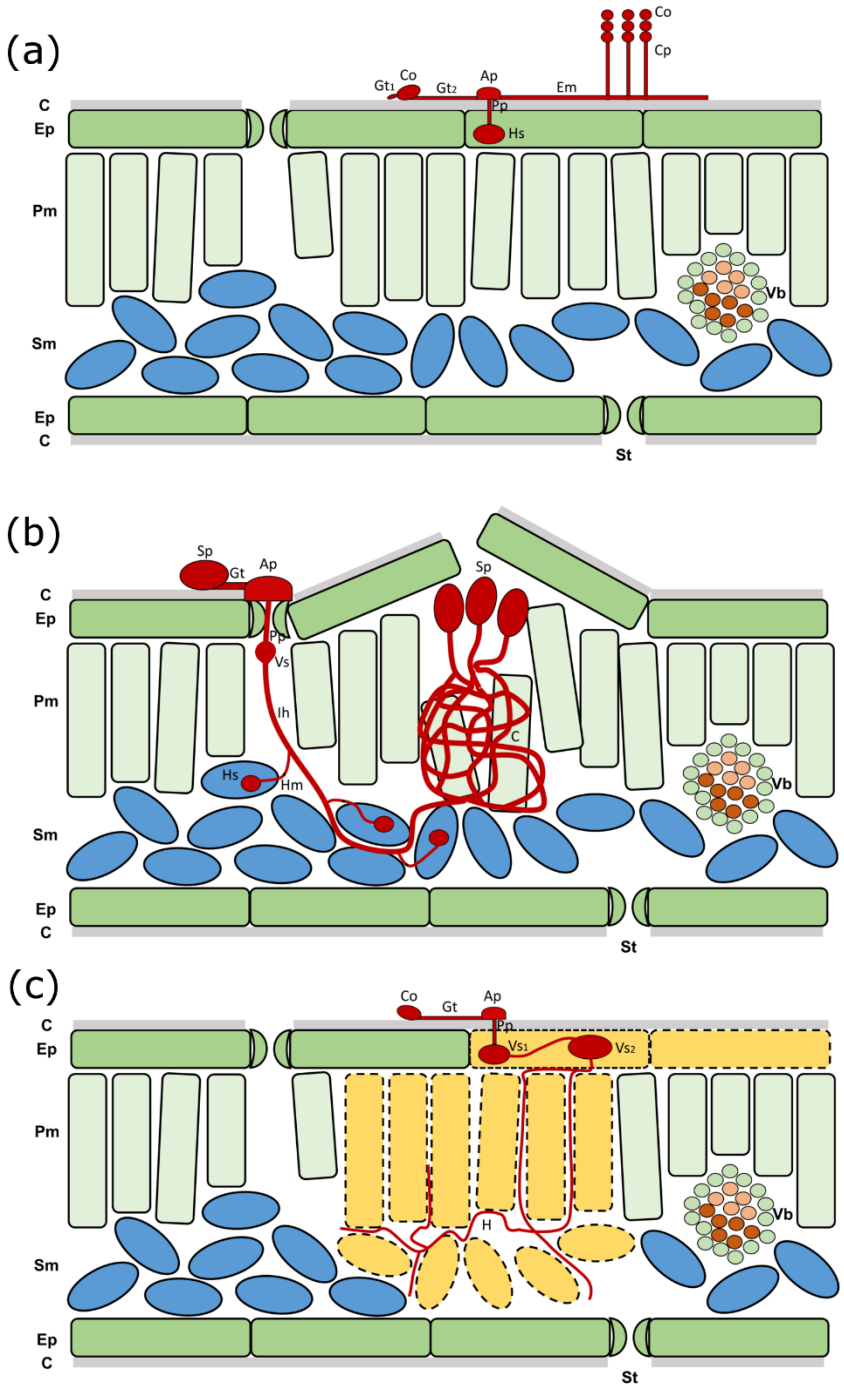

Fig. 2 Interactions of the pathogens *Blumeria graminis* f. sp. *hordei* (a), *Puccinia hordei* (b) and *Pyrenophora teres* f. *teres* (c) with barley leaves. C = cuticle, Ep = epidermis, Pm = palisade mesophyll, Sm = spongy mesophyll, St = stomata, Vb = vascular bundle, Co = conidia, Gt = germination tube, Ap = appressorium, Pp = penetration peg, Hs = haustorium, Em = epiphytic mycelia, Cp = conidiophores, Sp = Spore, Vs = vesicle, Ih = infection hypha, Hm = haustorial mother cell, C = colony, H = hyphae

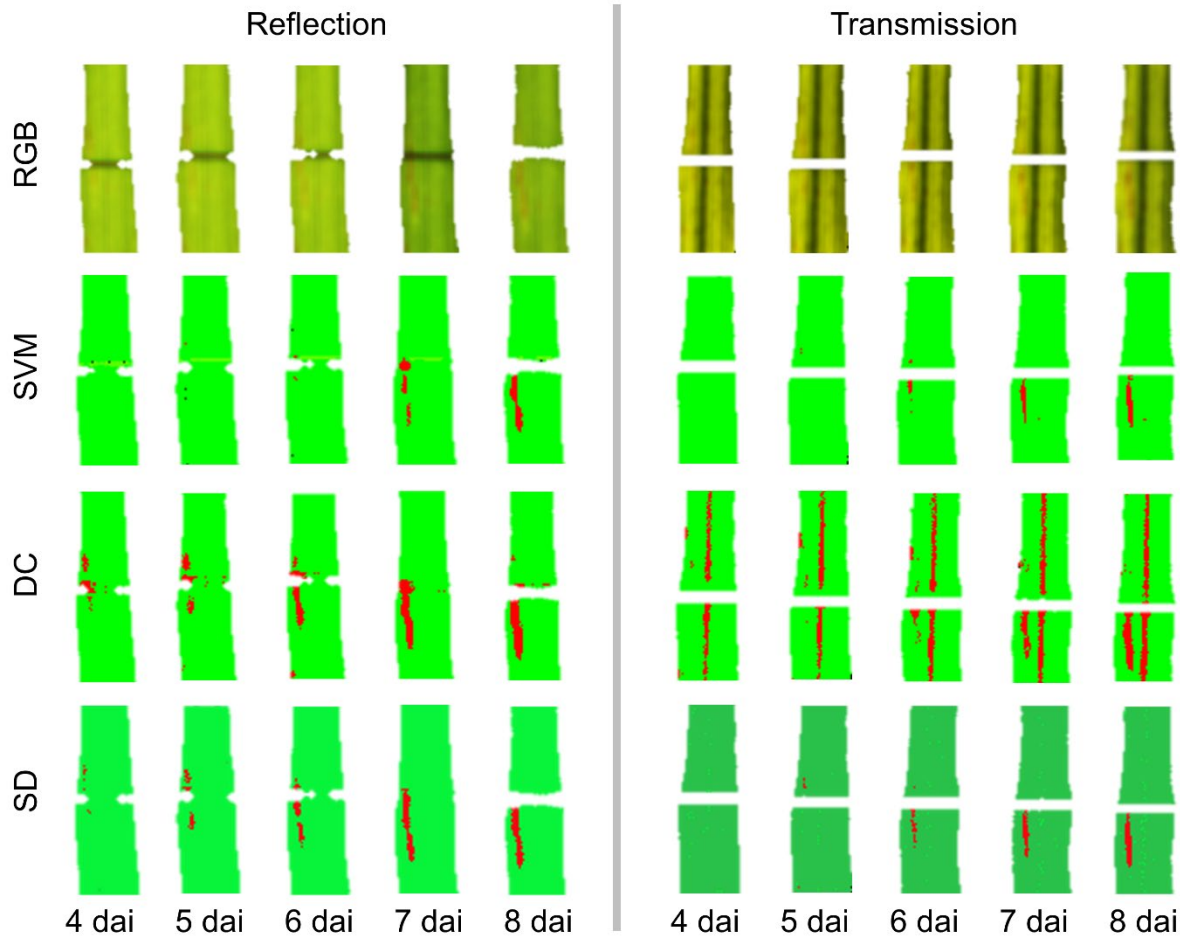

Fig. 3 Reflection and transmission images of an Ingrid wild type leaf, inoculated with *Pyrenophora teres* f. *teres* over the course of the experiment. The Pseudo RGB images are compared with false colour images, representing the classes healthy (green colours) symptom (red) and artefact (black) of the respective data analysis methods. RGB = Pseudo RGB, SVM = Support Vector Machines, DC = Distance Classifier, SD = Spectral Decomposition

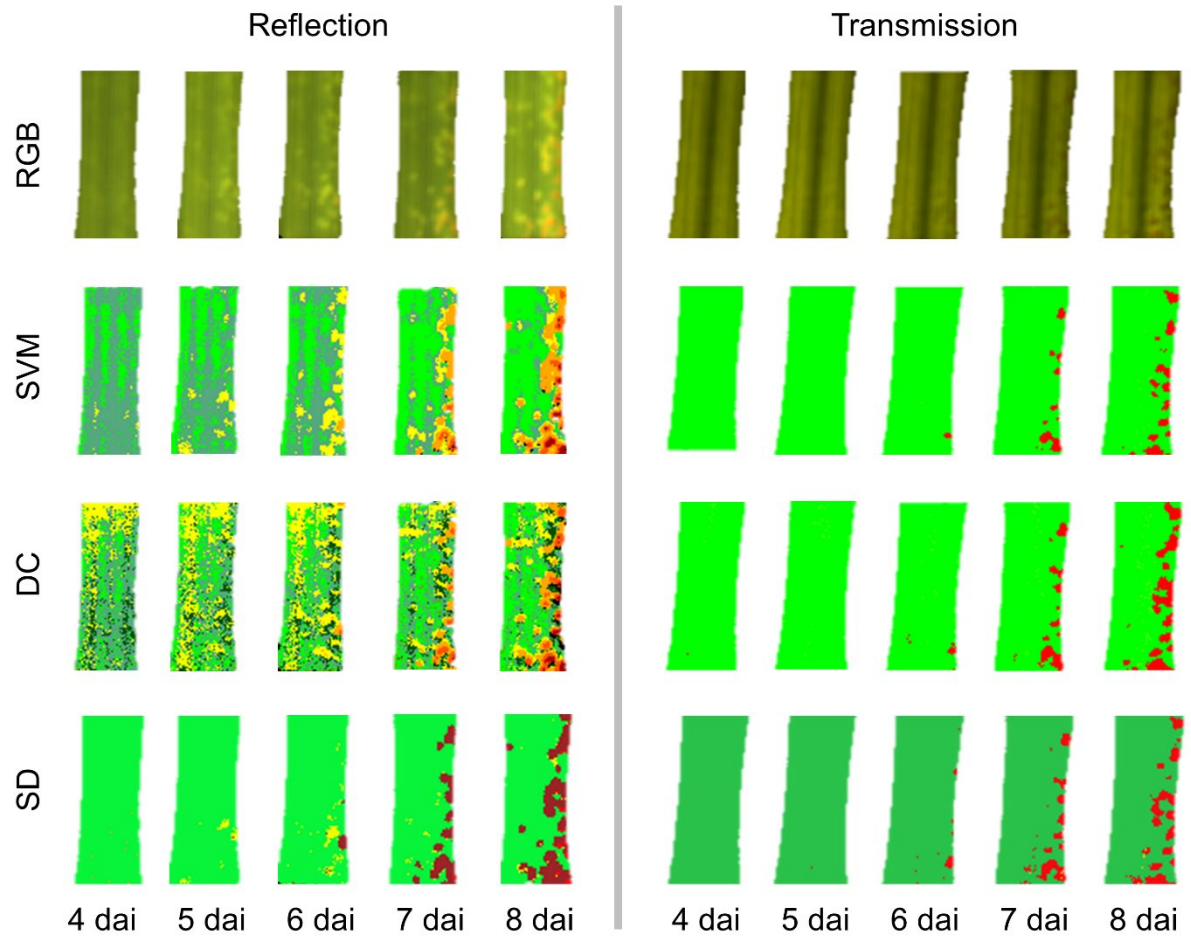

Fig. 4 Reflection and transmission images of an Ingrid wild type leaf, inoculated with *Puccinia hordei* over the course of the experiment. The Pseudo RGB images are compared with false colour images, representing the classes healthy (green colours) and symptom (yellow and red colours) of the respective data analysis methods. RGB = Pseudo RGB, SVM = Support Vector Machines, DC = Distance Classifier, SD = Spectral Decomposition

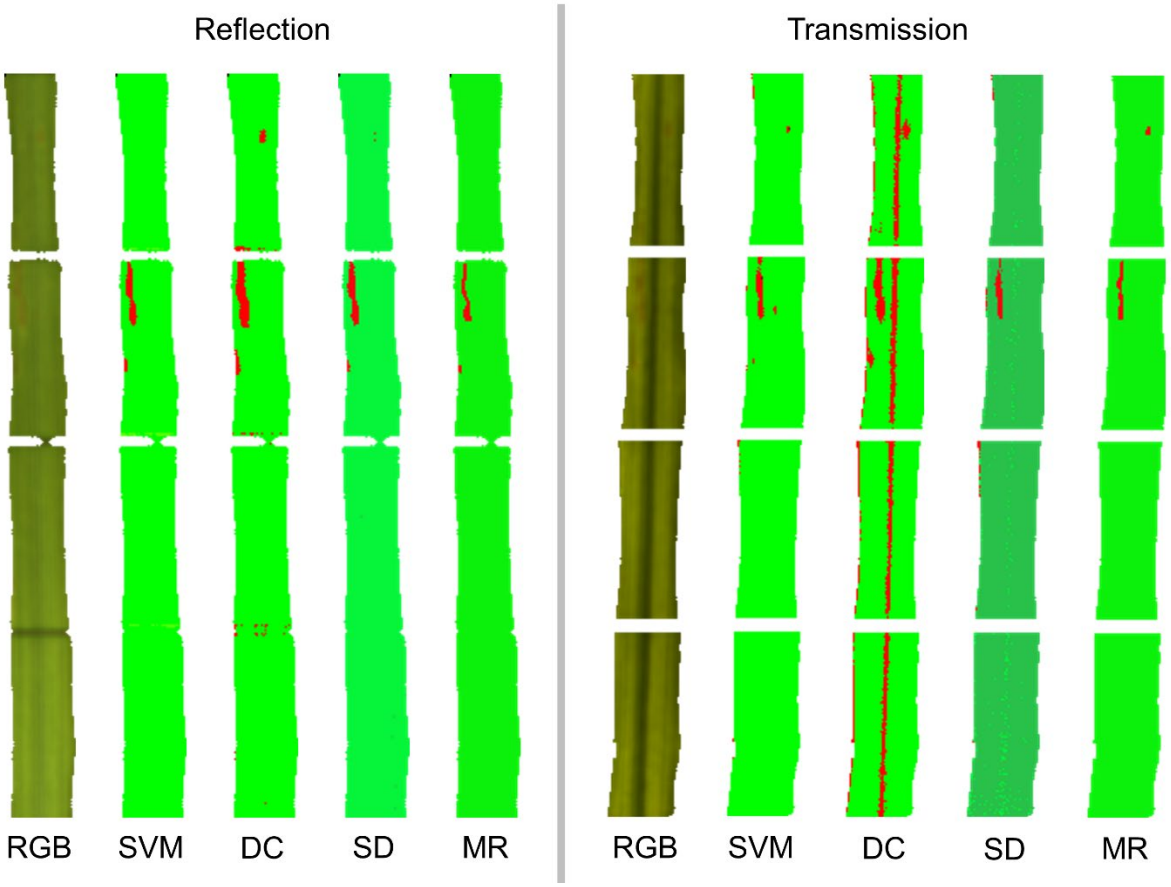

Fig. 5 Reflection and transmission image of an Ingrid wild type leaf, inoculated with *Pyrenophora teres* f. *teres* at 9 days after inoculation. The Pseudo RGB images are compared with false colour images, representing the classes healthy (green colours), symptom (red) and artefact (black) of the respective data analysis methods, as well as with the results of manual rating of the image by an expert. RGB = Pseudo RGB, SVM = Support Vector Machines, DC = Distance Classifier, SD = Spectral Decomposition, MR = Manual Rating

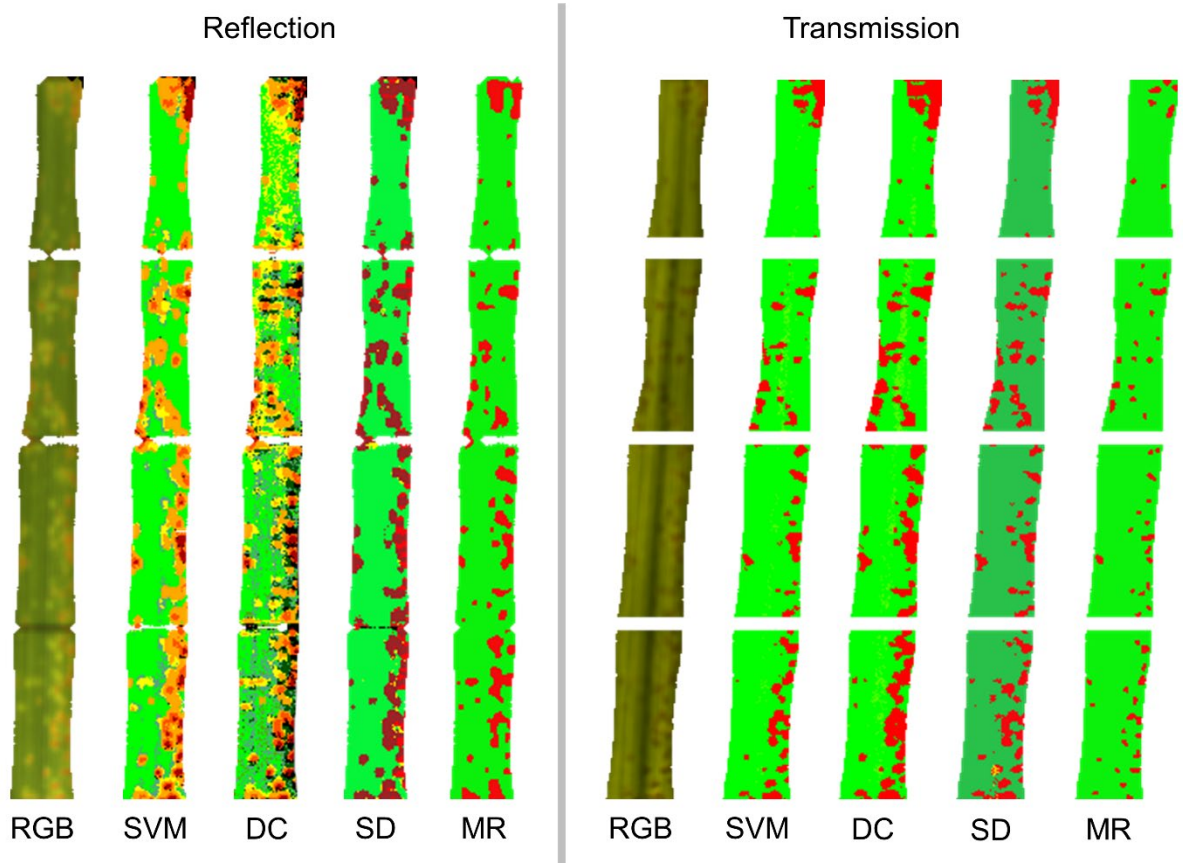

Fig. 6 Reflection and transmission image of an Ingrid wild type leaf, inoculated with *Puccinia hordei* at 9 days after inoculation. The Pseudo RGB images are compared with false colour images, representing the classes healthy (green colours) and symptom (yellow and red colours) of the respective data analysis methods, as well as with the results of manual rating of the image by an expert. RGB = Pseudo RGB, SVM = Support Vector Machines, DC = Distance Classifier, SD = Spectral Decomposition, MR = Manual Rating

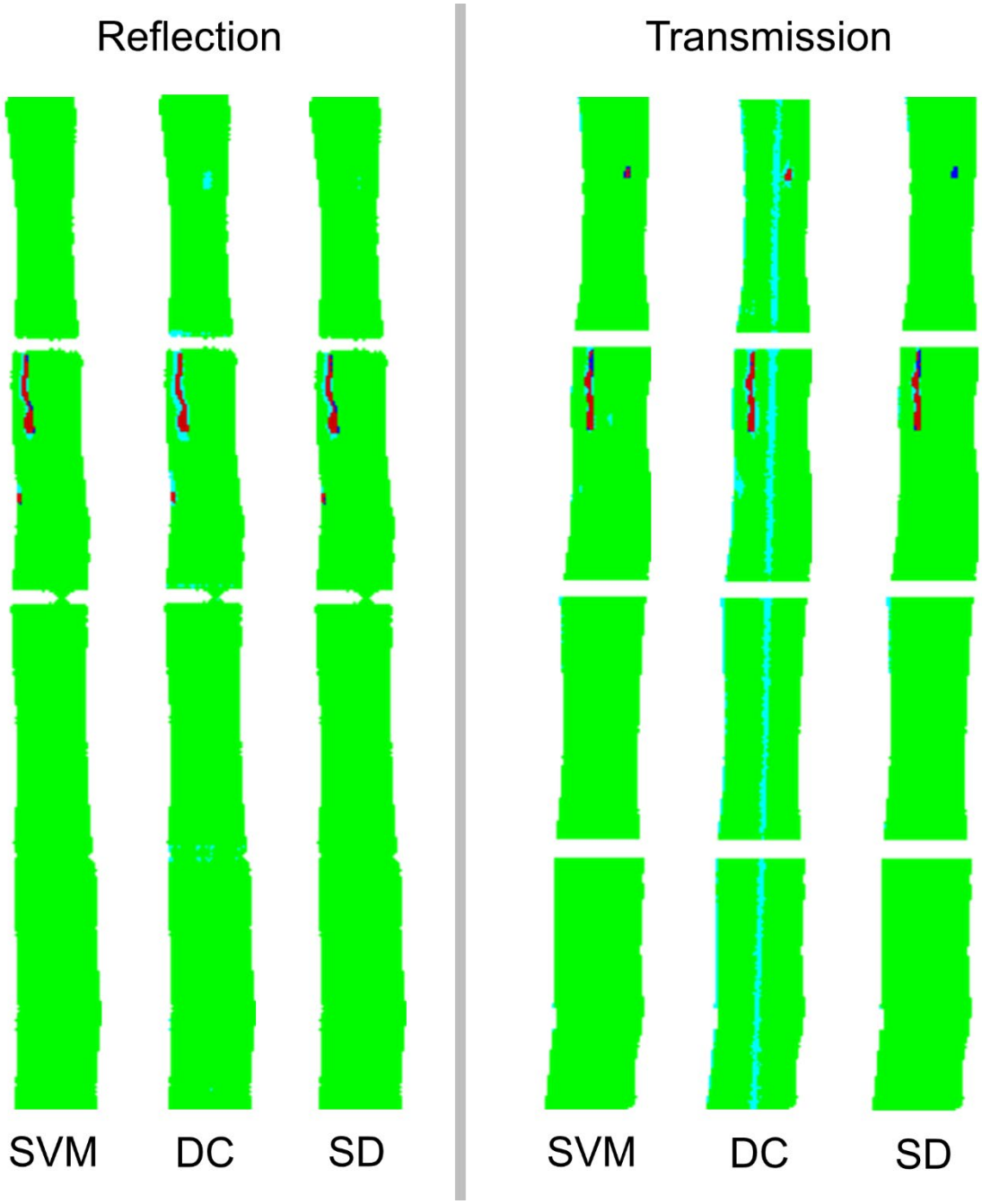

Fig. 7 False colour visual representation of confusion matrix results on net blotch infected leaves at 9 dai for reflection and transmission images. The images show the comparison of the respective data analysis method classification outcome compared to manual rating. Green and red pixels representing healthy and symptom classification which showed no difference for manual rating and classification. Light blue coloured pixels represent pixels which were classified as symptoms in the data analysis and healthy in the manual rating. Dark blue coloured pixels respectively represent pixels that were labelled as symptoms in the manual

769 rating and classified as healthy through the data analysis. SVM = Support Vector Machines,

770 DC = Distance Classifier, SD = Spectral Decomposition

771

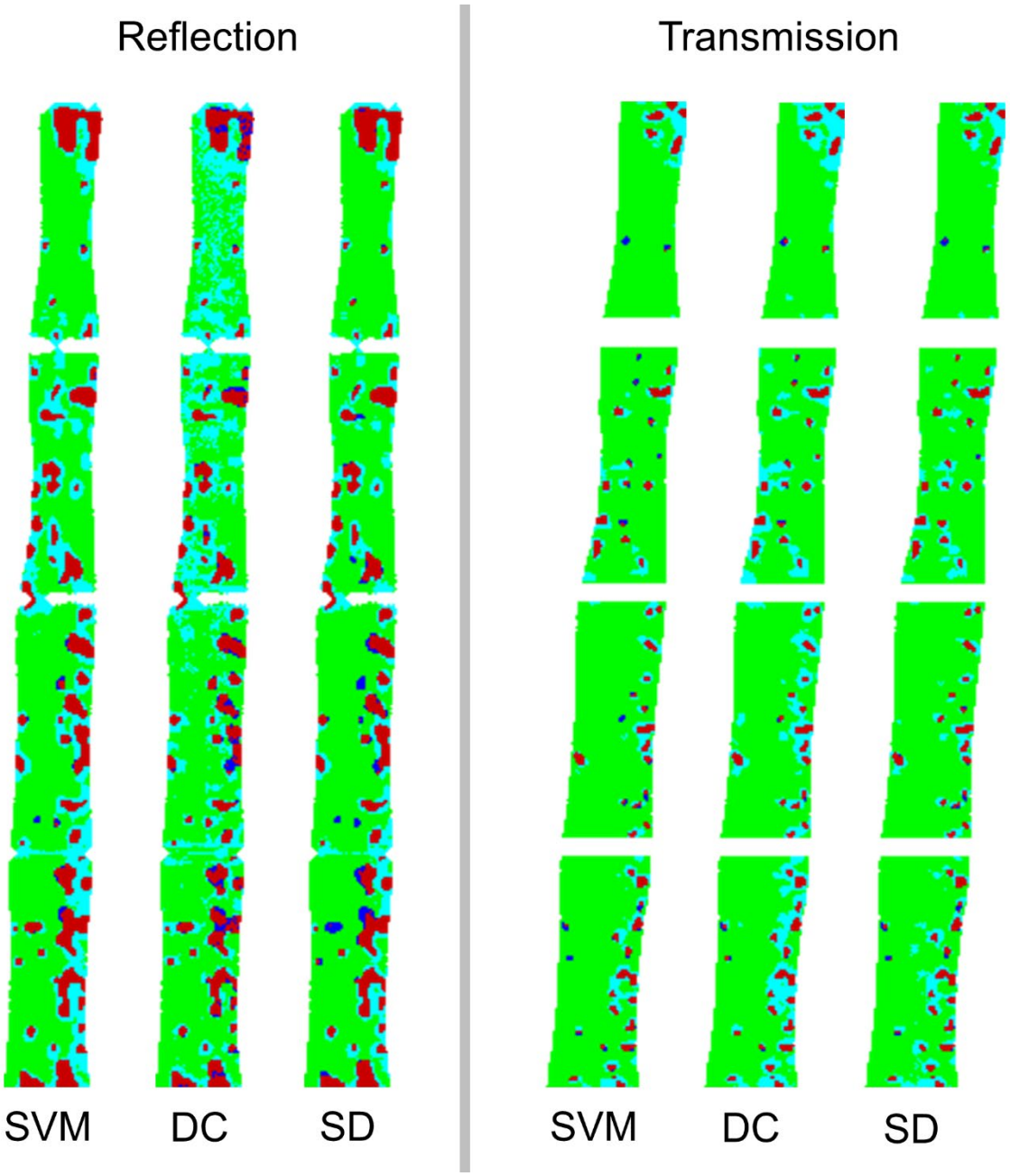

Fig. 8 False colour visual representation of confusion matrix results on brown rust infected leaves at 9 dai for reflection and transmission images. The images show the comparison of the respective data analysis method classification outcome compared to manual rating. Green and red pixels representing healthy and symptom classification which showed no difference for manual rating and classification. Light blue coloured pixels represent pixels which were classified as symptoms in the data analysis and healthy in the manual rating. Dark blue coloured pixels respectively represent pixels that were labelled as symptoms in the manual

780 rating and classified as healthy through the data analysis. SVM = Support Vector Machines,

781 DC = Distance Classifier, SD = Spectral Decomposition

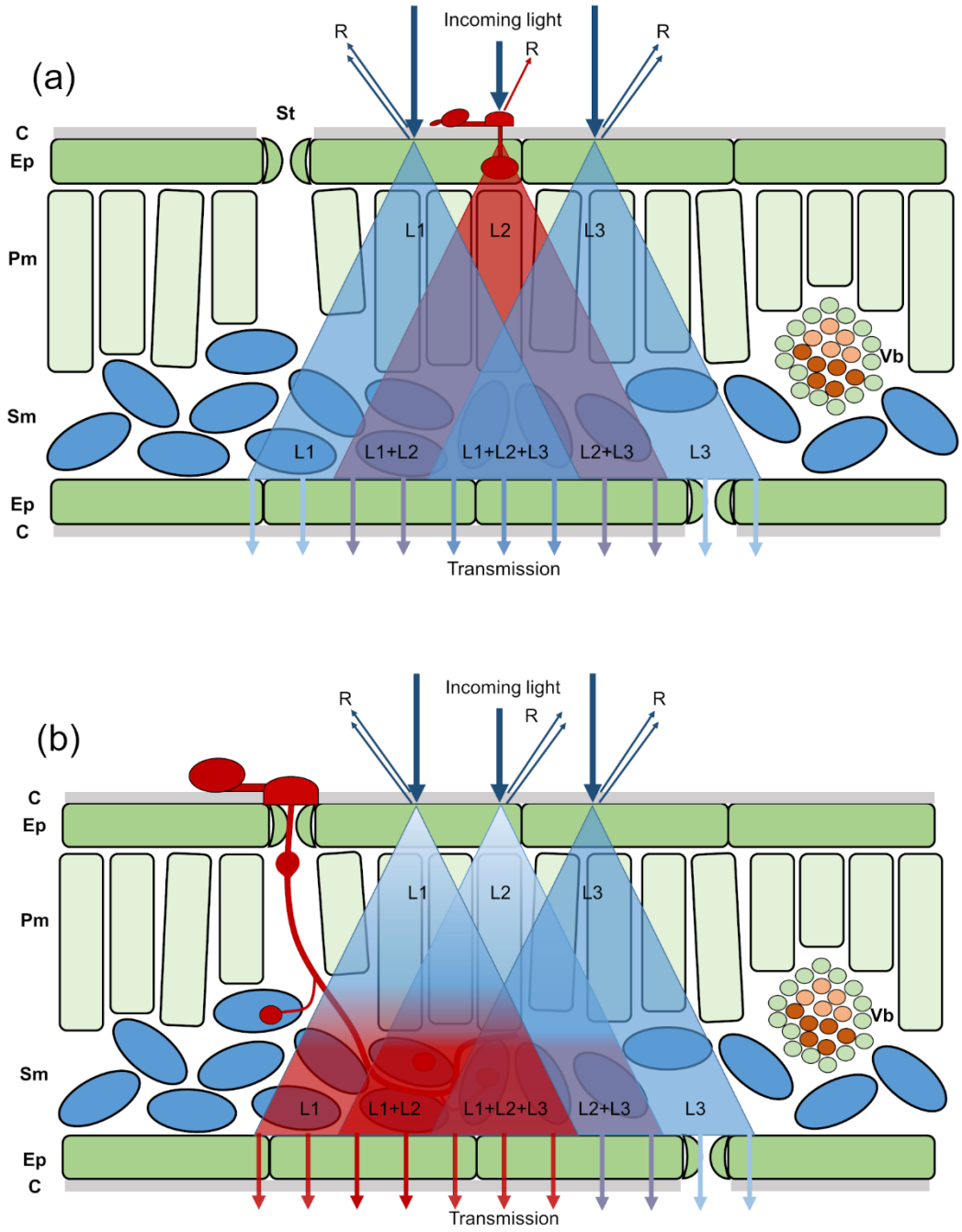

Fig. 9 Influence of diffuse light scattering inside plant leaf tissue for transmission-based measurement of pathogens which interact with the leaf surface and epidermis (Ep). Incoming light is colliding with the cuticle (C) and epidermis of the leaf, where a portion of the light is being directly reflected (R). This leads to a direct interaction of the reflected light with pathogens that grow on the leaf surface, resulting in a significant influence on the reflected lights wavelength. However, the portion of the light which is being transmitted through the leaf is being diffusely scattered (L1, L2, L3). For non-intrusive pathogens like powdery mildew (a) this leads to a significant overlap of light, which did not come in contact with the pathogen, when exciting the leaf tissue as transmitted light (L1+L2+L3). For more intrusive pathogens like brown rust (b) this effect is significantly reduced, as the light interacts with the pathogen in deeper plant tissue layers, thereby reducing the effect of the scattering on

detection accuracy for transmitted light. Pm = palisade mesophyll, Sm = spongy mesophyll, St = stomata, Vb = vascular bundle

Tables:

Table 1: Disease severity calculation of net blotch and brown rust inoculated leaves at 9 days after inoculation with different data analysis algorithms and comparison to manual rating. DC = Distance Classifier, SVM = Support Vector Machines, SD = Spectral Decomposition, r = reflectance, t = transmittance.

	Net blotch r.	Net blotch t.	Brown rust r.	Brown rust t.
Manual rating	0.72%	0.69%	15.25%	5.04%
SVM	1.04%	1.05%	35.92%	11.72%
DC	2.4%	11.18%	37.9%	20.75%
SD	1.12%	0.98%	27.35%	13.98%

804 Table 2: Results of confusion matrix on images classified with manual rating compared to the
805 applied data analysis methods for net blotch and brown rust infected leaves at 9 days after
806 inoculation. Values in percent represent the percentage of the total amount of pixels within the
807 respective classes, which were classified correctly based on the results of the manual rating.
808 DC = Distance Classifier, SVM = Support Vector Machines, SD = Spectral Decomposition.

			Manual Rating			
			Net blotch		Brown rust	
			Healthy	Symptom	Healthy	Symptom
Reflection	SVM	Healthy	99.6%	0.4%	74.2%	25.8%
		Symptom	10.4%	89.6%	3%	97%
	DC	Healthy	98.3%	1.7%	69.6%	30.4%
		Symptom	0%	100%	13.7%	86.3%
	SD	Healthy	99.4%	0.6%	83.5%	16.5%
		Symptom	15.5%	84.5%	11.7%	88.3%
Transmission	SVM	Healthy	99.5%	0.5%	92.2%	7.8%
		Symptom	21.6%	78.4%	14%	86%
	DC	Healthy	89.4%	10.6%	84.1%	15.9%
		Symptom	2.1%	97.9%	4.5%	95.5%
	SD	Healthy	99.5%	0.5%	90.2%	9.8%
		Symptom	29.9%	70.1%	7.7%	92.3%

809